PROCEEDINGS of the
23rd International Congress on Acoustics
9 to 13 September 2019 in Aachen, Germany

# Fast algorithms applied to the acoustical energy boundary element method

Matthias RAM[(1)], Otto VON ESTORFF[(1)]

[(1)]Hamburg University of Technology, Institute of Modelling and Computation, Germany, mub@tuhh.de

**Abstract**

The Energy Boundary Element Method (EBEM) aims at the solution of acoustic high frequency problems, where the classic BEM becomes inefficient due to the large number of degrees of freedom (DOF) required. A transition to non-phased energetic state variables removes the correlation between the investigated frequency range and the element size. In the EBEM the number of DOF is thus determined primarily by the complexity of the geometry. In order to speed up the computation and to handle structures of very high geometric complexity, a fast multipole algorithm for the EBEM is investigated. It has a great potential to reduce the numerical effort in the Boundary Element Method (BEM). Helmholtz and Laplace problems have been solved very efficiently applying this algorithm. However, the kernels used in the EBEM require an adaptation of the algorithm. In this paper the development of a fast multipole formulation of the EBEM is presented.

Keywords: Fast multipole, Boundary elements, Energy method

## 1 INTRODUCTION

Nowadays, the BEM can be considered a well-established solution technique for acoustic problems of many kinds. The number of a models DOF $N$ required for satisfactory solution accuracy, however, does not only depend on the complexity of the geometry, but also on the investigated frequency range. A commonly used rule of thumb suggests at least 6-10 elements per wave length. Since the matrices of the system of equations in the BEM are generally fully populated and non-symmetric, the memory required for the storage and solution, as well as the solution time, grow very fast with the maximum frequency under consideration. Thus, the BEM is mostly limited to the low and medium frequency ranges. The numerical effort for the conventional BEM grows proportionally with $\mathcal{O}\left(N^2\right)$. The application of the Fast Multipole Method (FMM) allows the reduction of the complexity to $\mathcal{O}\left(N\right)$ respectively $\mathcal{O}\left(N\log N\right)$ [1]. Although this improvement means a tremendous acceleration and considerably extends the frequency range where BEM is applicable, the FMM accelerated BEM (FMBEM) still fails to cover the entire audible frequency range in most practical problems.

The EBEM constitutes a different approach to deal with the particular challenges of high frequency problems [2, 3, 4, 5]. By neglecting interferences between propagative waves and using energetic quantities for the description of the sound field, similarly to the statistical energy analysis (SEA), the correlation between the investigated frequency and the element size is removed. To satisfy the underlying assumptions, the calculations have to be carried out within a broader frequency range that contains several eigenfrequencies. The method is thus only applicable for higher frequencies, where the modal overlap is high and yields a frequency-smoothed response. Unlike in the SEA, the results obtained by the EBEM give detailed insight in the local spatial distribution of the variables describing the sound field.

This paper aims at the formulation of a FMM for the EBEM (FMEBEM) to speed up the computation and allow for finer discretiziation, where it is required by high geometric complexity of the model. The approach, first presented in [6], is discussed in more detail. Section 2 gives an outline of general FMM procedures. In section 3 the application to the EBEM is shown followed by numerical experiments to verify the accuracy and performance of the FMEBEM presented in section 4. The paper closes with a summary and an outlook in section 5.

## 2 FUNDAMENTALS OF FMM ACCELERATED BOUNDARY ELEMENT METHODS

The following section is based on references [1, 7, 8] which may be consulted for more in depth information. The boundary integral equations occurring in the BEM are of the form

$$f(\mathbf{x}) = \int_\Gamma K(\mathbf{x},\mathbf{y})\phi(\mathbf{y})\,\mathrm{d}\mathbf{y} \qquad \mathbf{x} \in \Gamma, \tag{1}$$

where $\mathbf{x}$ and $\mathbf{y}$ denote the position of receiver and source point, respectively. The function $f$ is known on the boundary $\Gamma$ of the computational domain, $\phi$ is an unknown function and $K(\mathbf{x},\mathbf{y})$ is a given kernel function. The underlying idea of the FMBEM is to avoid the costly evaluation of all the direct interactions between separate elements when evaluating the kernel function. Instead, several neighboring source elements are clustered and their influence on sufficiently far situated receiver elements is evaluated by some suitable approximation resulting in a "post office scenario" as illustrated in Figure 1.


Figure 1. Direct evaluation of interactions (a) and evaluation in a single stage FMM (b) according to [7]

### 2.1 Definitions

The mathematical basis for the FMM is given by a factorization of the kernel function of the form

$$K(\mathbf{x},\mathbf{y}) = \sum_{n=0}^{\infty} k_n^{(1)}(\mathbf{x}-\mathbf{y}_0)k_n^{(2)}(\mathbf{y}-\mathbf{y}_0). \tag{2}$$

In Equation 2, $\mathbf{y}_0$ denotes an arbitrary point in the $\mathbb{R}^3$. The functions $k_n^{(1)}$ are usually singular in the origin, whereas $k_n^{(2)}$ are usually entire functions [1]. The separation of receiver and source in Equation 2 principally allows the desired clustering after truncation of the infinite series. The expansion, however, is usually valid under a certain condition only, the most common being

$$\|\mathbf{x}-\mathbf{y}_0\| > \|\mathbf{y}-\mathbf{y}_0\|. \tag{3}$$

To ensure this condition, a hierarchical tree structure is introduced. In 3D, a so called *oct-tree* is used. To obtain the tree, a cubic bounding box is defined, so that it contains the entire boundary surface. This bounding box is said to be on *level 0* and contains all the elements of the model. Boxes at higher levels $l > 0$ are created by splitting the *parent* box on level $l-1$ into eight equally sized *children*. The division is repeated until either a desired level or a limiting number of elements per box is reached. A childless box on the deepest level is called *leaf*. Furthermore the following definitions are introduced: Two boxes are said to be *near neighbors* if they are on the same level and share at least one boundary point. A box is within the *interaction list* of another box of the same level if their parents are near neighbors but the boxes themselves are not.
Boxes that are not near neighbors are well separated, meaning that Equation 3 is satisfied for all points of the receiving box when $\mathbf{y}_0$ is chosen as the center point of the box containing the source point. Thus, it becomes obvious that a tree structure in the FMM must always consist of at least three levels, since on level 0 and 1 there are no well separated boxes. At level 2 on the other hand, all well separated boxes are within the interaction list of a box and their influence can be taken into account by evaluation of Equation 2. If the depth of the tree exceeds level 2, the method at hand is called Multi Level Fast Multipole Method (MLFMM).

Using Equation 1 and Equation 2 a *multipole expansion* for $\Gamma_0$, the part of $\Gamma$ contained within the box, and a point $\mathbf{x}$ outside the box is obtained as

$$\int_{\Gamma_0} K(\mathbf{x},\mathbf{y})\phi(\mathbf{y})\,\mathrm{d}\mathbf{y} = \sum_{n=0}^{\infty} k_n^{(1)}(\mathbf{x}-\mathbf{y}_0)M_n(\mathbf{y}_0), \tag{4}$$

where the *multipole moment* centered at $\mathbf{y}_0$ is defined by

$$M_n(\mathbf{y}_0) = \int_{\Gamma_0} k_n^{(2)}(\mathbf{y}-\mathbf{y}_0)\phi(\mathbf{y})\,\mathrm{d}\mathbf{y}. \tag{5}$$

In a similar manner, a *local expansion* is defined for a point $\mathbf{x}$ inside a box as

$$\int_{\Gamma_0} K(\mathbf{x},\mathbf{y})\phi(\mathbf{y})\,\mathrm{d}\mathbf{y} = \sum_{n=0}^{\infty} L_n(\mathbf{x}_0)k_n^{(3)}(\mathbf{x}-\mathbf{x}_0), \tag{6}$$

where $L_n(\mathbf{x}_0)$ denotes the local coefficients centered at $\mathbf{x}_0$ and the functions $k_n^{(3)}$ are chosen to be a complete set of interior solutions of the governing partial differential equation. For obvious reasons, the summations in Equation 4 and 6 have to be truncated after a finite number of terms in practical implementations.
To complete the tool set for the MLFMM, three operators are required: An operator to shift the center of a multipole expansion from a box to its parent, called *M2M*, an operator to translate a multipole expansion centered at a box to a local expansion centered at another box in its interaction list, which is called *M2L* and an operator to shift the center of a local expansion from a box to its child, called *L2L*.

### 2.2 Algorithm

The FMM can be employed for the approximation of a matrix-vector product and as such in combination with an iterative solver for the solution of a boundary value problem by means of the BEM. The major steps of the procedure are as follows. First, the boundary is discretized and a trial vector is determined as usual. The elements are organized in a tree structured as described in subsection 2.1. Starting at the deepest level, the multipole moments for all leaf boxes are calculated using Equation 5. The multipole moments are then shifted to the respective parent boxes using *M2M*, summing up the contributions of all the children of a parent. This procedure is repeated following the hierarchy of the tree upwards until all boxes on level 2 posses a multipole moment. Once this step is completed, the multipole moments on each level are translated to local coefficients of the interaction list using *M2L* and summed up for each box. Now, starting from level 2, tracing the tree downwards, the local coefficients of each parent box are shifted to its children using *L2L* and are added to their existing coefficients. Once again, this step is repeated until all leaf boxes posses a local expansion that accounts for the influence of all well separated boxes. This expansion is then evaluated using Equation 6. The contributions of all source points within the same box and near neighbor boxes are evaluated directly and are added to the result from the local expansion.

## 3 APPLICATION OF THE FMM TO THE EBEM

The boundary integral equation used in the EBEM is [3, 5]

$$\int_{\Gamma} \mathbf{H}(\mathbf{x},\mathbf{y})\cdot\mathbf{n}_x\sigma(\mathbf{y})\,\mathrm{d}\mathbf{y} + c(\mathbf{x})\sigma(\mathbf{x}) = I_n(\mathbf{x}). \tag{7}$$

In Equation 7, $\mathbf{n}_x$ denotes the outward normal vector at the receiving point, $\sigma$ the source strength on the boundary, $c(\mathbf{x})$ the boundary factors and $I_n(\mathbf{x})$ the sound intensity in normal direction. The kernel function is given by

$$\mathbf{H}(\mathbf{x},\mathbf{y}) = \frac{e^{-\mu r}}{4\pi}\frac{\mathbf{r}}{r^3}, \tag{8}$$

where $\mathbf{r} = \mathbf{x} - \mathbf{y}$, $r = \|\mathbf{x} - \mathbf{y}\|$ and $\mu$ is the attenuation coefficient. The strong singularity occurring in Equation 8 may be handled by a suitable numerical integration scheme [9]. In case of constant elements these singularities are avoided. To apply the FMM to Equation 7 an expansion in the form of Equation 2 for Equation 8 is required. In its general form, no obvious factorization of the kernel function seems to be available. Since the kernel is not oscillatory and smooth outside the singularity, the application of a so called kernel-independent or black box FMM [11] would be feasible, where the factorization does not need to be explicitly known. For the special case $\mu = 0$, however, which is a valid assumption for many practical problems, an analytical formulation as described in section 2 can be found. This analytical FMM for the undamped case will be described in the following. As $\mu = 0$, the following identity is observed

$$\mathbf{H}(\mathbf{x},\mathbf{y}) \cdot \mathbf{n}_x = \frac{\mathbf{r} \cdot \mathbf{n}_x}{4\pi r^3} \equiv -\frac{\partial G(\mathbf{x},\mathbf{y})}{\partial \mathbf{n}_x}. \tag{9}$$

where $G(\mathbf{x},\mathbf{y}) = \frac{1}{4\pi r}$ denotes the Green's function of Laplace's equation. Thus, the scalar product $\mathbf{H}(\mathbf{x},\mathbf{y}) \cdot \mathbf{n}_x$ is taken as the negative normal derivative of the Laplace kernel function at the receiver point. With this approach, a FMM based on the factorization of $G(\mathbf{x},\mathbf{y})$, known as [10]

$$G(\mathbf{x},\mathbf{y}) = \frac{1}{4\pi} \sum_{n=0}^{\infty} \sum_{m=-n}^{n} \bar{S}_n^m(\mathbf{x} - \mathbf{y}_0) R_n^m(\mathbf{y} - \mathbf{y}_0), \tag{10}$$

is possible. In Equation 10 the symbol $\bar{\cdot}$ indicates the complex conjugate. The functions $R_n^m$ and $S_n^m$ are known as regular and singular *solid harmonics*. They are defined in terms of the polar coordinates $r, \phi, \theta$ of a vector $\mathbf{x}$ as

$$R_n^m(\mathbf{x}) = \frac{1}{(n+m)!} P_n^m(\cos\theta) e^{\mathrm{i}m\phi} r^n \tag{11}$$

and

$$S_n^m(\mathbf{x}) = \frac{1}{(n-m)!} P_n^m(\cos\theta) e^{\mathrm{i}m\phi} \frac{1}{r^{n+1}}, \tag{12}$$

where $P_n^m$ is the associated Legendre function of degree $n$ and order $m$. Here, the definition of $P_n^m$ from [10] is used, where the factor $(-1)^m$, known as Condon-Shortley phase, is omitted from the definition. By comparing Equation 10 to Equation 2 it becomes obvious that $k_l^{(1)}(\mathbf{x} - \mathbf{y}_0) = \bar{S}_{n(l)}^{m(l)}(\mathbf{x} - \mathbf{y}_0)$ and $k_l^{(2)}(\mathbf{y} - \mathbf{y}_0) = R_{n(l)}^{m(l)}(\mathbf{y} - \mathbf{y}_0)$ have been chosen, where the original summation index $n$ has been replaced with $l$ to avoid confusion with associated Legendre functions degree $n$.

The normal derivative appearing in Equation 9 depends on the receiver position only. Due to the separation of source and receiver, its computation requires a modification of the last step of the FMM algorithm only, which is the evaluation of at the receiver position by Equation 6. Using

$$k_l^{(3)}(\mathbf{x} - \mathbf{x}_0) = \frac{\partial R_{n(l)}^{m(l)}(\mathbf{x} - \mathbf{x}_0)}{\partial \mathbf{n}_x}, \tag{13}$$

Equation 6 can be rewritten as

$$\int_{\Gamma_0} \mathbf{H}(\mathbf{x},\mathbf{y}) \cdot \mathbf{n}_x \sigma(\mathbf{y})\, \mathrm{d}\mathbf{y} = -\frac{1}{4\pi} \sum_{n=0}^{\infty} \sum_{m=-n}^{n} L_n^m(\mathbf{x}_0) \frac{\partial R_n^m(\mathbf{x} - \mathbf{x}_0)}{\partial \mathbf{n}_x}. \tag{14}$$

Taking the discretization into account, the multipole moment of the leaf boxes may be calculated from the elements $i$ inside the box with their shape functions $N_i$ as

$$M_n^m(\mathbf{y}_0) = \sum_{i \in Box} \int_{\Gamma_i} R_n^m(\mathbf{y} - \mathbf{y}_0) N_i(\mathbf{y}) \sigma(\mathbf{y})\, \mathrm{d}\mathbf{y}. \tag{15}$$

The operators *M2M*, *M2L* and *L2L* can be adopted from the FMM for the Laplace equation. These are [10]

$$M_n^m(\mathbf{y}_0') = \sum_{n'=0}^{n} \sum_{m'=-n'}^{n'} R_{n'}^{m'}(\mathbf{y}_0 - \mathbf{y}_0') M_{n-n'}^{m-m'}(\mathbf{y}_0), \tag{16}$$

$$L_n^m(\mathbf{x}_0) = \sum_{n'=0}^{\infty} \sum_{m'=-n'}^{n'} (-1)^n \bar{S}_{n+n'}^{m+m'}(\mathbf{x}_0 - \mathbf{y}_0) M_{n'}^{m'}(\mathbf{y}_0), \tag{17}$$

$$L_n^m(\mathbf{x}_1) = \sum_{n'=n}^{\infty} \sum_{m'=-n'}^{n'} R_{n'-n}^{m'-m}(\mathbf{x}_1 - \mathbf{x}_0) L_{n'}^{m'}(\mathbf{x}_0). \tag{18}$$

Where Equation 16 represents *M2M*, *M2L* is given by Equation 17 and Equation 18 defines *L2L*. For the evaluation of Equation 14 the derivatives of $R_n^m$ need to be calculated. They are given by [10]

$$\frac{\partial}{\partial x} R_n^m = \frac{1}{2}\left(R_{n-1}^{m-1} - R_{n-1}^{m+1}\right), \tag{19}$$

$$\frac{\partial}{\partial y} R_n^m = \frac{\mathrm{i}}{2}\left(R_{n-1}^{m-1} + R_{n-1}^{m+1}\right), \tag{20}$$

$$\frac{\partial}{\partial z} R_n^m = R_{n-1}^m. \tag{21}$$

As has been mentioned before, the expansion is truncated, thus the outer sum is terminated after $p$ terms, resulting in a total $p^2$ coefficients for the local and multipole expansion of each box. The number of terms $p$ is refered to as *expansion length*.

## 4 RESULTS

The previously described FMEBEM was implemented within the framework of a C++ library for acoustic boundary element analyses. The method was implemented as a MLFMM, where the number of levels $n_l$ is chosen according to [12] by

$$n_l \approx \log_8(N). \tag{22}$$

### 4.1 Sphere

For a first verification and to perform some numerical experiments concerning the performance and accuracy of the method, the geometry of a sphere is analyzed. Boundary conditions for the normal intensity are chosen such that they correspond to a point source in the center of the sphere. The sphere is modeled using 9,359 elements and constant shape functions. In Figure 2, the resulting source strengths on the boundary are shown as computed by the direct evaluation of the boundary integral equation (Figure 2a) and the FMEBEM (Figure 2b-2e).

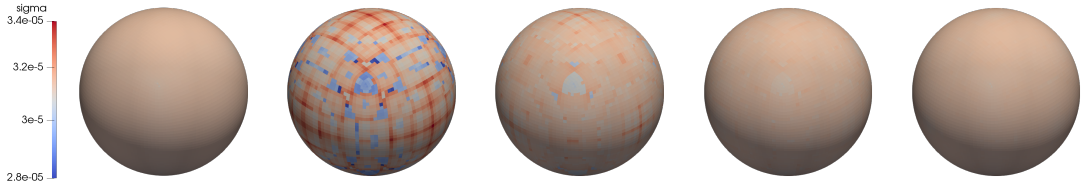


(a) direct EBEM (b) FMEBEM, $p = 3$ (c) FMEBEM, $p = 4$ (d) FMEBEM, $p = 5$ (e) FMEBEM, $p = 6$

Figure 2. Source strength on the boundary computed by direct evaluation of Equation 7 (a) and FMM with varying expansions lengths (b-e)

Using the expansion length $p = 3$, there are clearly visible artifacts in the solution, showing deviations from the direct solution within the order of magnitude of roughly 10 %. With increasing expansion length, however, these deviations decline and for $p = 6$ the results of the FMEBEM match those of direct computation very well. The operators *M2M*, *M2L* and *L2L* that have been implemented are of the complexity $\mathcal{O}\left(p^4\right)$, hence the expansion length can have great impact on the computation times and thus the efficiency of the FMM. To analyze the effect of the expansion length on accuracy and speed of the method in more detail, the mean relative error was calculated as

$$\varepsilon = \frac{\sqrt{\sum_N \left(\sigma_{\text{direct}}\left(r_i\right) - \sigma_{\text{FMM}}\left(r_i\right)\right)^2}}{\sqrt{\sum_N \sigma_{\text{direct}}^2\left(r_i\right)}}. \tag{23}$$

In Equation 23, $\sigma_{\text{direct}}\left(r_i\right)$ denotes the source strength at collocation point $i$ as computed by the direct EBEM and $\sigma_{\text{FMM}}$ the source strength as a result of the FMM. The resulting error as well as the required computation times are shown in Figure 3. The behavior of the error for large $p$ is unexpected. From theory, a monotonously

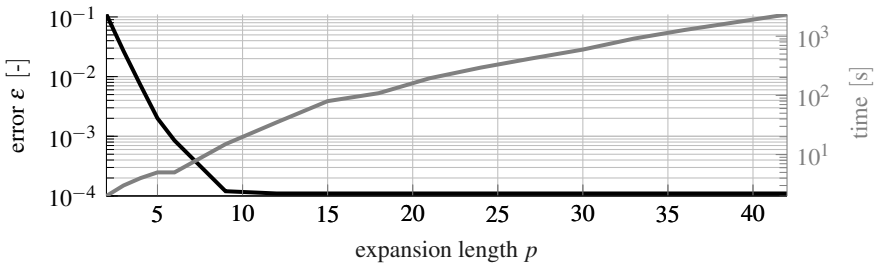


Figure 3. Computing time and relative error of the FMEBEM over the expansion length

decreasing error, that eventually converges towards zero would be expected. However, the error in Figure 3 converges towards a finite value. The reason for this behavior is suspected to be related to inaccurate handling of very large numerical values occurring during the computation of the factorials in Equation 11 and 12 for large $p$. Since the overall accuracy is still good and the effect only occurs for impractically large expansion lengths, it was not yet further investigated.

To analyze the performance of the method for varying problem sizes, the sphere was discretized with approximately 1,000 elements. This base mesh was refined several times by splitting the element edges until a maximum of approximately one million elements was reached. Figure 4 shows the computing time and required memory for different numbers of DOF for both, direct EBEM and FMEBEM, using a constant expansion length of $p = 5$.

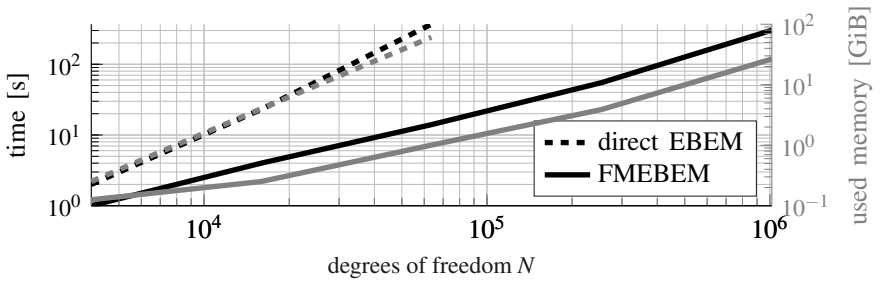


Figure 4. Computing time and memory consumption during solution for EBEM and FMEBEM for different problem sizes

It can be observed that the EBEM does scale approximately with the complexity $\mathcal{O}\left(N^2\right)$ while the FMEBEM behaves as $\mathcal{O}\left(N\right)$. The reduced effort allows for faster solution and larger problem sizes due to reduced memory consumption.

### 4.2 Car interior

Finally, a somewhat more complex model has been analyzed to demonstrate the applicability to more realistic engineering problems. The mesh shown in Figure 5 was used to model a generic car interior excited by a loudspeaker system. It consists of approximately 40,000 constant elements. The blue circular area in the front has a unit intensity defined as boundary condition, modeling a uniformly vibrating speaker membrane. For the green area at the bottom a high absorption coefficient of $\alpha_{floor} = 0.7$ is defined. The remaining yellow elements have a low absorption of $\alpha = 0.05$ prescribed. While there are severe simplifications in comparison to an actual car interior, the complexity of the model is high compared to the sphere since different types of boundary conditions and a more complex geometry are involved. Solutions computed by EBEM (6a) and FMEBEM using $p = 5$ (6b) are shown in Figure 6. The results match very well, though the relative error computed on the

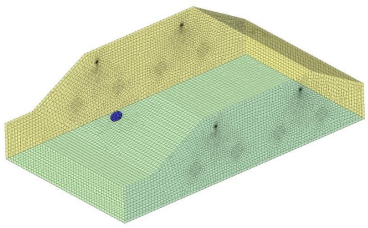

Figure 5. Model of a generic car interior

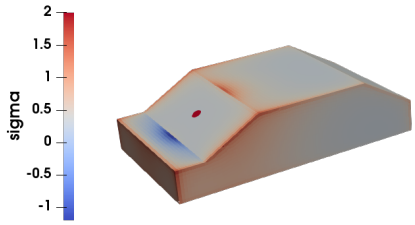


(a) EBEM solution

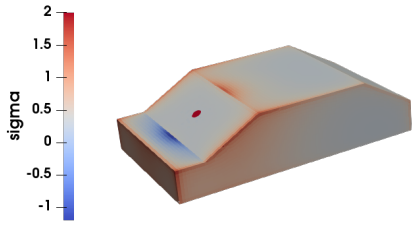


(b) FMEBEM solution

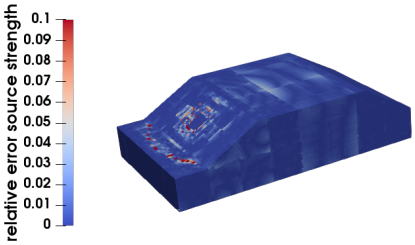


(c) error on the boundary

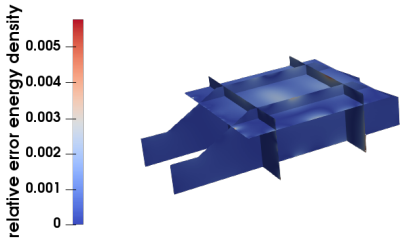


(d) error inside the domain after post processing

Figure 6. Comparison of solutions for the car model obtained by EBEM and FMEBEM

boundary (6c) becomes quite large in some areas. However, the areas, where the largest relative error occurs, are those, where the EBEM solution approaches zero so even very small absolute errors result in large relative errors. The evaluation of the field variables after post processing the results (6d) shows excellent agreement.

## 5 SUMMARY AND OUTLOOK

A fast multipole method for the undamped EBEM kernel function has been developed and analyzed. The method has been verified by results of a direct EBEM and shows very high accuracy. The required memory during the solution is reduced significantly and speed is vastly increased compared to the direct evaluation.
More efficient operators of complexity $\mathcal{O}\left(p^3\right)$ are known for the Laplace kernel [1, 10, 12]. They offer the potential to improve the current implementation. The application of a black box FMM for the damped and undamped EBEM kernel [11] may also be of interest.

## REFERENCES


[1] Nishimura, N. Fast multipole accelerated boundary integral equation methods, Applied Mechanics Reviews 55 (4), 2002, pp 299-324

[2] Bitsie, F. The Structutral-Acoustic Energy Finite Element Method and Energy Boundary Element Method, Dissertation, Purdue University, 1996

[3] Le Bot, A. A Vibroacoustic Model for High Frequency Analysis, Journal of Sound and Vibration 211, 1998, pp 537-554

[4] Wang, A.; Vlahopoulos N.; Wu, K. Development of an energy boundary element formulation for computing high-frequency sound radiation from incoherent intensity boundary conditions, Journal of Sound and Vibration 278, 2004, pp 413-436

[5] Ram, M.; Keuchel, S.; Piepiorka, J.; von Estorff, O. Energiebasierte BEM und Fast-Multipole BEM für Hochfrequenzprobleme: Eine Gegenüberstellung, Fortschritte der Akustik - DAGA 2018, 19.-22. März 2018 in Munich

[6] Ram, M.; Keuchel, S.; von Estorff, O. Beschleunigungsverfahren für die Energie-Boundary-Elemente-Methode, Fortschritte der Akustik - DAGA 2019, 18.-21. März 2019 in Rostock

[7] Gumerov, N. A.; Duraiswami, R. Fast Multipole Methods for the Helmholtz Equation in Three Dimensions, Elsevier Series in Electromagnetism, Elsevier Science, 2004

[8] Keuchel, S. Aufwandsreduzierung in der Fast-Multipole-Boundary-Elemente-Methode, Technische Universität Hamburg-Harburg, 2017

[9] Keuchel, S.; Hagelstein, N. C.; Zaleski O.; von Estorff, O. Evaluation of hypersingular and nearly singular integrals in the Isogeometric Boundary Element Method for acoustics, Computer Methods in Applied Mechanics and Engineering 325, 2017, pp 488-504

[10] Yoshida, K.-I. Applications of Fast Multipole Method to Boundary Integral Equation Method, Kyoto University, 2001

[11] Fong, W.; Darve, E. The black-box fast multipole method, Journal of Computational Physics 228 (23), 2009, pp 8712-8725

[12] Greengard, L.; Rokhlin, V. A New Version of the Fast Multipole Method for the Laplace Equation in Three Dimensions, Research Report YALEU/DCS/RR-1115, 1996